Ultra-low thermal conductivity in Cs-Sb-Se compounds: Lattice instability vs. lone-pair electrons

Saikat Mukhopadhyay[1*], David J. Singh[2] and Thomas L. Reinecke[3*]

[1]NRC Research Associate at Naval Research Laboratory, Washington, DC 20375

[2] Department of Physics and Astronomy and Department of Chemistry, University of Missouri, Columbia, Missouri 65211

[3]Naval Research Laboratory, Washington, DC 20375

*Corresponding Author: SM:saikatrel@gmail.com, TLR:tom.reinecke@nrl.navy.mil

ABSTRACT

Lone-pair electrons (LPE) are known to lead to large anharmonicity in materials and thus to low lattice thermal conductivity (κ). Materials with LPE typically have lower κ than those with similar compositions but without LPE. In this study, we investigate thermal transport properties in Cs-Sb-Se ternary compounds by first principles methods and show that LPE do not necessarily guarantee the lowest κ. We find that the calculated κ in LPE free Cs_3SbSe_4 is smaller (~0.1 W/mK) than κ in $CsSbSe_2$ (~0.3W/mK), which has LPE. This is unusual and contradictory to the traditional concept where LPE leads to low κ. We explain this discrepancy in terms of the local structural instabilities. The small ionic radius of Sb^{5+} brings the Se^{2-} close to one another. This leads to a large Coulomb repulsion between them making the $[SbSe_4]^{3-}$ polyhedra in Cs_3SbSe_4 unstable and results in soft phonons and high thermal displacements for the Sb and Se for this material. This gives large anharmonicity and higher scattering rates in Cs_3SbSe_4 than that from the LPE-driven anharmonicity of $CsSbSe_2$.

Thermoelectrics provide scalable solid-state energy conversion as well as fascinating challenges in materials science. As such, they have been the focus of much recent interest in energy technology, and this in turn has driven important discoveries in the science of thermal transport in solids. One example is the connection between lone pair electrons and low lattice thermal conductivity [1,2,11–15,3–10] . This is important for realizing high thermoelectric performance through low thermal conductivity, and it impacts other areas including piezoelectrics and perovskite solar cell materials [16,17]. Ideal candidates for thermoelectric applications are materials that allow the electrons to move freely (high electrical conductivity; σ) but inhibit the propagation of phonons giving low thermal conductivity (κ) and an enhanced figure of merit; $zT = \sigma S^2 T/\kappa$, where S is the Seebeck coefficient and T is absolute temperature. Therefore, detailed understanding of the mechanisms that inhibit phonon propagation through materials is important for designing materials for thermoelectric applications. Low group velocities and high scattering rates arising from large anharmonicity are common in materials that exhibit low κ. Long bond-lengths (weakly bonded systems) generally lead to the low group velocities, however, a number of mechanisms including bonding inhomogeneity [18,19], local distortion [20], phonon-nesting [21], twisting modes [22] and resonant bonding [23] are reported to yield large anharmonicity resulting in low κ.

Phonons play a key role in carrying heat in (crystalline) semiconductors, and their frequencies and interactions are determined by the underlying electronic structure, including the bonding. One example of current interests concerns the effects of lone-pair electrons (LPE). It has been shown in a series of materials [1,2,11–15,3–10] that s^2 LPE lead to low κ except some cases of 2D materials [24]. This is because the s^2 lone-pair electrons make the lattice more prone to deformation in the presence of lattice vibration, leading to soft phonons and anharmonicity. A number of reports have studied different phases of materials with the same constituent atoms and concluded that phases with LPE typically lead to lower κ as compared to those without LPE. For example, among phases of Cu-Sb-Se compounds, $CuSbSe_2$ and Cu_3SbSe_3 have lower κ than Cu_3SbSe_4 because of enhanced anharmonicity due to the Sb^{3+} lone-pair electrons[2,6]. A number of studies confirmed this finding for ABX_2 (A=Na, K, Rb, Cs; B= As, Sb, Bi; X=S,Se)[1,9,25] materials where the LPE from the B-atoms created large anharmonicity and soft modes (low-group velocities)

leading to low κ. Thus, LPE have become a useful chemical design-rule for finding new low thermal conductivity compounds.

In this work, we investigate the thermal transport properties of Cs_3SbSe_4 and $CsSbSe_2$. The Sb^{3+} lone-pair electrons in $CsSbSe_2$ could be expected to lead to a lower κ compared to Cs_3SbSe_4, which does not have such lone pairs. However, we find that Cs_3SbSe_4 has lower κ (~0.1 W/m-K) than $CsSbSe_2$ (~0.3 W/m-K) at room temperature. This is uncommon and in contrast to the well-established understanding of LPE-driven low κ. We then compared the structural and lattice dynamical properties of Cs_3SbSe_4 to those of $CsSbSe_2$ using first principles methods to find the origin of this anomalous κ behavior of Cs_3SbSe_4 in terms of its crystal chemistry.

Results: The predicted structures obtained from the density functional calculations as implemented in Materials Project [26] are shown in Fig. 1. Both compounds show similar stabilities with equal (zero) convex hull distances (the formation energy difference between the target compound and its competing phases) on a compositional phase diagram (Fig. S1 in Supporting Information; SI). This indicates that both compounds are thermodynamically stable at 0 K. Cs_3SbSe_4 has space group type, *Pnma* (# 62). This structure is similar to that of alkali metal chalcogenometallates with a K_3VS_4-type structure[27]. There are two crystallographically independent Cs^+ cations in the asymmetric unit. The Cs-1 ions are fivefold coordinated by the Se atoms of five $[SbSe_4]^{3-}$ polyhedrons whereas Cs-2 ions are sevenfold coordinated by seven Se atoms from four $[SbSe_4]^{3-}$ units with irregular polyhedra [Fig. 1(a)]. These units contain Sb^{5+} ions stabilized by the coordinating Se anions, which therefore do not involve lone pairs. The average Csl-Se distance is 3.82 Å and average Cs2-Se distance is 3.76 Å. The Sb atoms form tetrahedrons with average Sb-Se distance = 2.52 Å. $CsSbSe_2$ has space group type $P2_1/c$ (# 14)[28]. The average Cs-Se bond distances are 3.75 Å whereas the average Sb-Se bond distances in the $[SbSe_2]^{1-}$ polyhedrons are 2.98 Å. These polyhedral units are based on Se coordination of Sb^{3+} ions, which implies LPE chemistry.

Cs_3SbSe_4 is a direct-gap semiconductor with a gap of ~1.5 eV and $CsSbSe_2$ is an indirect band-gap semiconductor with band gap of ~1 eV. The top of the valence band of Cs_3SbSe_4 is largely dominated by the Cs-p orbitals with minor Sb-p contributions, reflecting the ionic nature of the compound. The valence band for $CsSbSe_2$ is comprised of Se-p with contributions from Sb-p and

Sb-s orbitals. These Sb-s orbitals are reported to be repelled by the Se-p electrons resulting in soft lattice with large anharmonicity. In addition, the Cs atoms are weakly bonded in both the Cs_3SbSe_4 and $CsSbSe_2$ with long average bond-lengths connecting to the nearest neighbor atoms; 3.87 and 3.75Å. These nearly non-bonded Cs atoms are expected to give low-frequency optic modes.

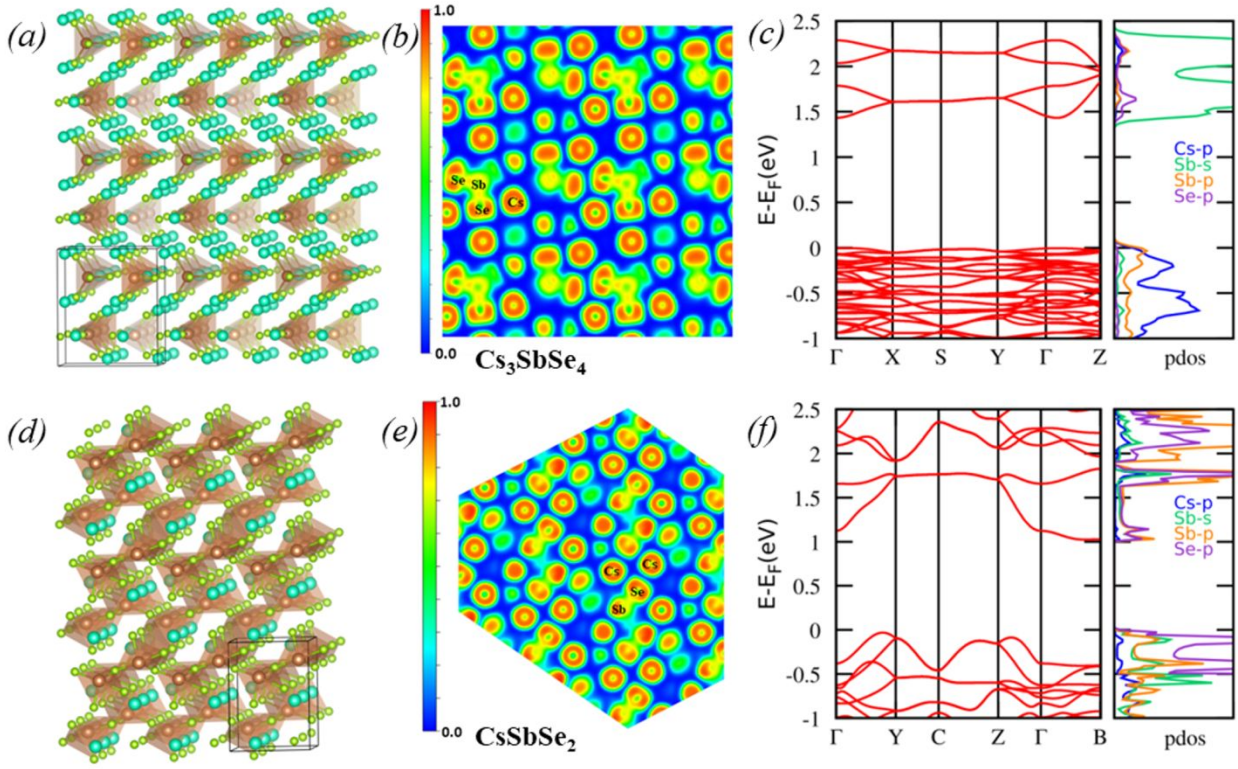

Figure 1: Structural and electronic properties: (a) and (d): $3 \times 3 \times 3$ *supercells of* Cs_3SbSe_4 *and* $CsSbSe_2$ *where Cs, Sb and Se atoms are represented by aqua, orange and lime-green spheres. The corresponding unit cells are represented by boxes with solid black lines. (b) and (e): Electron localization functions projected along the [101] and [111] plane of* Cs_3SbSe_4 *and* $CsSbSe_2$. *(c) and (f): Electron band structures with the density of states projected on the orbitals for* Cs_3SbSe_4 *and* $CsSbSe_2$.

We calculated κ for the two compounds as a function of temperature from direct solution to the phonon Boltzmann transport equation (Fig. 2). Both compounds have low thermal conductivities that can be associated with the weak bonding of these Cs compounds. The phonon contribution to κ in Cs_3SbSe_4 is very low (0.1 W/mK) approaching κ in molecular crystals [29,30]. Commonly known low κ materials including Zintl-phase Eu_2ZnSb_2 [31], Half-Heuslers[32], skutterudites [33,34],

clathrates [35] and materials with complex unit cells such as $Gd_{117}Co_{56}Sn_{112}$ [36] and $CsAg_5Te_3$[37] exhibit higher κ than that in Cs_3SbSe_4 as shown in Fig. 2.

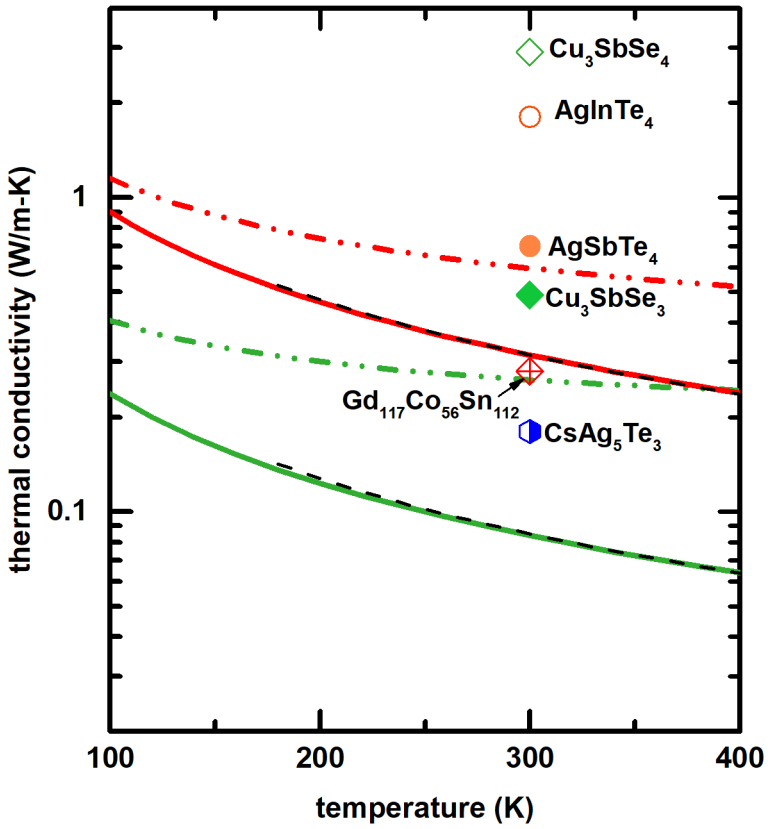

Figure 2: Calculated thermal conductivities in Cs_3SbSe_4 (solid green line) and $CsSbSe_2$ (solid red line) with their corresponding T^{-1}asymptotics (black dashed lines). The corresponding calculated thermal conductivities from the two-channel model (discussed below) are given in dashed-dotted green and red lines. The measured κ for Cu_3SbSe_3 and Cu_3SbSe_4[6], $AgSbTe_4$ and $AgInTe_4$[38] are shown as representative systems showing κ in systems with/without LPE. The measured κ for $Gd_{117}Co_{56}Sn_{112}$ [36] and $CsAg_5Te_3$ [37] represents known low κ materials with very complex unit cells.

The calculated κ in Cs_3SbSe_4 is unusual compared to that in $CsSbSe_2$ (Fig. 2). $CsSbSe_2$ has same constituent atoms as in Cs_3SbSe_4 and is expected to exhibit large anharmonicity because of its LPE. However, the calculated lattice κ in Cs_3SbSe_4 is smaller (κ ~ 0.1 W/mK) than that in $CsSbSe_2$ (κ ~ 0.3 W/mK). This is in contrast to previous studies where LPE resulted in the lowest κ among all the material-phases. For example, κ in LPE-free Cu_3SbSe_4[6] and $AgInTe_4$[38] (open

symbols in Fig. 2) were found to be higher than that in Cu_3SbSe_3[6] and $AgSbTe_4$[38] (filled symbols), respectively, which have active LPE.

To understand the origin of the calculated low κ in Cs_3SbSe_4, we focus on the phonon band structure and phonon anharmonicity in Cs_3SbSe_4 and compare them with those in $CsSbSe_2$. Calculated phonon dispersions and corresponding average phonon group velocities show anisotropy due to structural anisotropies along different crystal directions in Cs_3SbSe_4 and $CsSbSe_2$ as shown in Fig. 3. Since the acoustic phonons are the major heat carriers in these cases, the anisotropy in the calculated κ (Fig. S2) can be explained in terms of different group velocities of the acoustic phonons along different crystal directions as seen in the phonon dispersion (Fig. 3). The average group velocities in $CsSbSe_2$ are higher than those in Cs_3SbSe_4 (Fig. 3.c) due to relatively shorter bond lengths (stronger bonding) in $CsSbSe_2$ than in Cs_3SbSe_4. Longer bonds give softer lattices with lower group velocities and are often associated with larger anharmonicity. Therefore, the lower group velocities due to weaker bonds in Cs_3SbSe_4 than in $CsSbSe_2$ play an important role in causing lower κ in Cs_3SbSe_4.

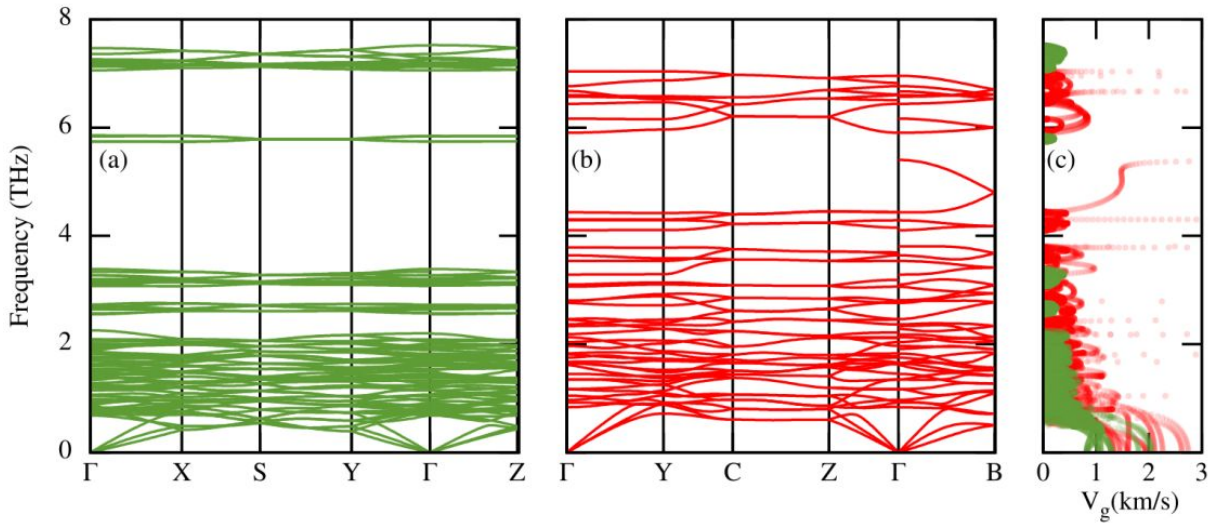

Figure 3: Phonon dispersion of (a) Cs_3SbSe_4 and (b) $CsSbSe_2$. (c) Calculated average group velocities for Cs_3SbSe_4 (in green) and $CsSbSe_2$ (in red).

Low κ in Cs_3SbSe_4 stems from its giant large anharmonicity that results in large phonon scattering rates. The anharmonic scattering rates for Cs_3SbSe_4 and $CsSbSe_2$ at room temperature

are shown in Fig. 4. The three phonon scattering rates in Cs_3SbSe_4 are higher than those in the commonly known anharmonic systems such as SnTe [39,40], PbTe [40,41], and PbS [23] where scattering rates are lower than 1THz [23]. Scattering rates in Cs_3SbSe_4 are also higher than those derived from the LPE-driven large anharmonicity in $CsSbSe_2$ (Fig. 4 (c-d)).

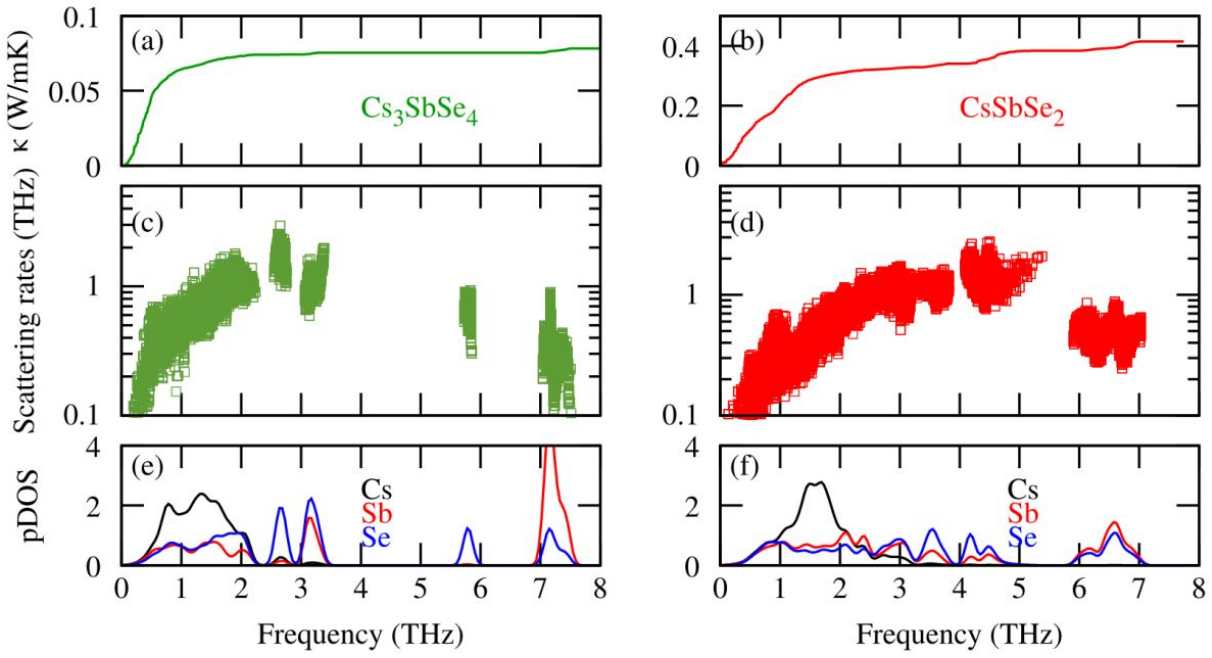

Figure 4: Accumulated κ at 300K as a function of frequency for (a) Cs_3SbSe_4 and (b) $CsSbSe_2$. Scattering rates as a function of frequency for (c) Cs_3SbSe_4 and (d) $CsSbSe_2$ at 300K. Phonon density of states (pDOS/atom) projected on constituent atoms for (e) Cs_3SbSe_4 and (f) $CsSbSe_2$.

The accumulated κ in Cs_3SbSe_4 and $CsSbSe_2$ (Fig. 4 (*a-b*)) gives further insight into the phonon scattering processes. The accumulated κ in Cs_3SbSe_4 and $CsSbSe_2$ increases with frequency as more phonons start to contribute to the total κ and then changes slope around 0.6-1.0 THz for Cs_3SbSe_4 and 1.0-1.5 THz for $CsSbSe_2$. Subsequently, the accumulated κ saturates, and flattens out at higher frequency due to low phonon group velocities of optic branches (flat bands) and enhanced scattering rates. Therefore, phonons around these frequency ranges in both the systems are responsible in suppressing κ. For Cs_3SbSe_4, the lowest-frequency optic mode (0.6 THz) plays an important role in enhancing the anharmonicity leading to the first peak in the scattering rates at 0.6 THz [Fig. 4(c)]. On the other hand, first peak in the scattering rates at 1THz for $CsSbSe_2$ comes from the higher frequency optic modes (not the lowest-frequency optic mode at 0.8THz).

The differences in scattering processes in Cs_3SbSe_4 and $CsSbSe_2$ can be understood from the nature of three phonon interactions. We show the mode-dependent three-phonon phase space as a function of frequency in Fig. S3. Phonon phase space represents the available scattering channels for phonons satisfying energy and momentum conservation and is directly proportional to the three-phonon scattering rates (Fig. 4). The phase space available for the absorption processes ($\lambda + \lambda' \rightarrow \lambda''$) in Cs_3SbSe_4 is larger than that in $CsSbSe_2$ [Fig. S3 (a)] whereas the phase space associated with emission processes ($\lambda'' \rightarrow \lambda + \lambda'$) is larger in $CsSbSe_2$ than in Cs_3SbSe_4 [Fig. S3(b)]. The low-frequency acoustic phonons are mainly scattered by the low-frequency optical modes via the absorption processes while the optic modes decompose largely into low energy acoustic modes in the emission process ($\lambda'' \rightarrow \lambda + \lambda'$). The dispersive nature of the lowest-frequency optic mode in Cs_3SbSe_4 enables it to satisfy the conservation laws for the absorption processes involving low frequency acoustic modes leading to higher phase space (Fig. S3 (a)) and to higher scattering rates (Fig. 4) than in $CsSbSe_2$. The lowest-frequency optic mode in $CsSbSe_2$ is less dispersive, which explains the smaller phase space associated with it and leads to lower scattering rates than in Cs_3SbSe_4. The change in the slope seen in the accumulated κ for $CsSbSe_2$ can be explained in terms of the high emission processes involving the optic modes with frequencies > 1 THz as shown in Fig. S3 (b). Therefore, we conclude that the origin of large anharmonicity in Cs_3SbSe_4 is associated with the strongly anharmonic lowest frequency optic mode whereas $CsSbSe_2$ derives its anharmonicity from higher-frequency optic phonon modes.

We now turn to the characteristic features of the lowest-frequency optic modes. The lowest-frequency optic mode in Cs_3SbSe_4 is dominated by the vibration of weakly bonded Cs atoms with some contributions of the Sb and Se atoms (Fig. 4c). This B_{3g} mode represents an uncorrelated rocking motion of two crystal-subunits involving two symmetrically independent Cs atoms (see video V1 in SI). The lowest-frequency optic mode in $CsSbSe_2$ (A_u mode) represents stretching and anti-stretching vibrations of Cs, Sb and Se atoms contributing equally to the mode. Although characteristically different, the lowest-frequency optic modes in both the systems come from Cs, Sb, Se atoms. However, the optic mode in Cs_3SbSe_4 is more anharmonic than in $CsSbSe_2$. To see this, the mean square displacements (MSDs) of the atoms at room temperature are shown in Fig. S4. The MSD for Cs atoms is higher in Cs_3SbSe_4 (0.05 $Å^2$) than in $CsSbSe_2$ (0.03$Å^2$). This is expected because the weaker Cs bonds with longer bond lengths in Cs_3SbSe_4 make it easier to move the atoms from their equilibrium positions during the vibration

than in $CsSbSe_2$. However, the MSDs associated with the Sb and Se atoms in Cs_3SbSe_4 are higher than those in $CsSbSe_2$ although the average Sb-Se bond lengths are shorter in Cs_3SbSe_4 than in $CsSbSe_2$. This can be understood in terms of the stability of $[SbSe_4]^{3-}$ polyhedra obtained from the ionic radius of the Sb and Se atoms. The sum of the ionic radius of Sb^{5+} [0.74 Å] and Se^{2-} [1.84 Å] (here we use Shannon crystal radii) ions is 2.58 Å. This is slightly longer than the average Sb-Se bond distances [2.52 Å] in Cs_3SbSe_4 and is consistent with the ionic characterization from the band structure. However, the geometry brings the Se^{-2} close to one another resulting in a large Coulomb repulsion and making these polyhedra less stable. To balance this repulsion, the Se atoms move from their symmetric positions in a way that keeps the Sb-Se distances same but changes the Se-Sb-Se bond angles. This is reflected in the bond angle variance (2.6659°^{2}) and quadratic elongation (~1.001), a quantitative measure of distortion in coordination polyhedral[42]. These distorted polyhedra are more susceptible to deformation in the presence of lattice vibrations giving rise to high MSDs. In contrast, the average Sb-Se bond distances (2.98 Å) in $CsSbSe_2$ are longer than the sum of the ionic radius of Sb^{+3} [0.9 Å] and Se^{-2} [1.84 Å] ~2.74 Å, and the Sb has lower coordination in this compound. Therefore, the Sb-Se units in $CsSbSe_2$ are more stable than in Cs_3SbSe_4. Thus we conclude that although there is large anharmonicity in $CsSbSe_2$ derived from the Sb^{+3} lone-pair electrons, Cs_3SbSe_4 has softer and more anharmonic modes due to local structural instability.

Large anharmonicity and the low phonon group velocities in both of these systems leads to short phonon mean free paths (MFPs) that are comparable with the atomic bond distances. As shown in Fig. S5, the MFPs of some of phonons are less than the *Ioffe-Regel* limit[43] (average atomic bond distances). Thus the phonon Boltzmann transport equation is likely to breakdown for some of the phonons. For such systems a *two-channel model* [44] has been used to describe κ. In this model, κ-contributions that come from the phonons with MFPs below the *Ioffe-Regel* limit are removed and compensated by adding κ from localized oscillators; κ_{hop} [7,44]. The *two-channel model* gives an average κ = 0.26 and 0.6 W/mK for Cs_3SbSe_4 and $CsSbSe_2$ as shown in Fig 2. In addition to the *two-channel model*, Simoncelli *et al.* proposed a general transport equation where κ associated with the off-diagonal (coherences; κ_C) Wigner distribution was calculated to be 0.3W/m-K for $CsPbBr_3$[45]. This is very similar to κ_{hop}~0.34 W/mK from the localized oscillators within the *two-channel model* [44]. Therefore, κ_{hop} can be considered as a simplistic approximation

of the term κ_C in Ref.[45]. Xia *et. al.* [46] showed that finite-temperature renormalization of the low-frequency phonon modes enhances κ (and MFP) by reducing scattering rates and therefore, better explained the measured κ [46]. However, this approach is computationally expensive and is beyond the scope of this study because it required consideration of quartic anharmonicity. A similar approach was proposed by Ravichandran and Broido [47].

Experimental data for the thermal properties of Cs_3SbSe_4 and $CsSbSe_2$ are not currently available. For the present purposes of calculating thermoelectric properties we use the calculated κ-values from the *two-channel model*, which has been shown previously[44] to represent an upper bound to κ. These κ values, should give a lower bound for thethermoelectric figure of merit *zT* . Calculated Seebeck coefficients and *zT* as functions of p-type carrier concentration are given in Fig. S6. The peak-values for *zT* at 300K are 0.67 and 0.72 (Fig. S6 (b)) for a reasonable carrier concentration for Cs_3SbSe_4 and $CsSbSe_2$. These values result from their low κ and high Seebeck coefficients. We used a constant relaxation time ($\tau = 9 \times 10^{-14}$ s) to calculate *zT*. This is consistent with a previous study[48] where similar τ values were used for semiconductors with moderate band gaps. These *zT* values are encouraging considering these systems are free of toxic elements unlike the cases with Tl-based materials [7,44], Bi_2Te_3 and their derivatives[49].

Summary and Conclusions: We address the commonly held association of lone pair electrons (LPE) with low thermal conductivities (κ) in materials using first-principles methodologies. We consider two phases of Cs-Sb-Se ternary compounds and show that the LPE-free Cs_3SbSe_4 has a lower κ than $CsSbSe_2$, which has LPE. We find that although $CsSbSe_2$ has large anharmonicity associated with Sb^{3+} LPE, Cs_3SbSe_4 has even higher anharmonicity and lower κ arising from the local structural instability. Small Sb^{5+} ionic radius (and short Sb-Se bond distances) brings the Se^{2-} of $[SbSe_4]^{3-}$ closer to one another causing large Coulomb repulsion that displaces the Se^{2-} ions from their symmetric positions. This results in distorted $[SbSe_4]^{3-}$ polyhedra with bond angle variance and quadratic elongation. These distorted polyhedra are susceptible to deformation in the presence of lattice vibrations, which lead to an unstable local crystal sub-lattice with large Sb- and Se-thermal displacements that suppress κ. This study shows that local crystal instabilities regardless of their origin can efficiently suppress κ. These results provide guidance for designing new low κ materials for thermal barrier coatings, efficient thermoelectrics and

conversely in increasing the thermal conductivity of materials such as piezoelectrics where LPE are needed for their functional behavior.

Computational Methods: The structure of Cs_3SbSe_4 was determined using Materials Project[26]. The structure exhibited a stable configuration according to the conformational phase diagram (Figure S1 in the supporting information (SI)) with an energy above hull per atom of 0 eV. The internal coordinates as well as the volume of the unitcell were optimized using an energy cutoff of 400 eV employing projector augmented wave (PAW) method[44] within the generalized gradient approximation (GGA) of Perdew, Burke and Ernzerhof [45] as implemented in VASP[44,46]. We used PBE to investigate the lattice dynamics in $CsSbSe_2$ to be consistent with our structural calculation of Cs_3SbSe_4. However, the PBE-derived phonon dispersion had one of the TA modes that was parabolic along the Γ-B direction. This is unphysical for bulk materials such as $CsSbSe_2$. The LDA-derived phonon dispersion gives reasonable dispersion for the TA modes. A comparison of PBE/LDA phonon dispersion is shown in Fig. S7 in the SI. The phonon dispersions obtained using GGA and LDA are qualitatively similar with slightly softer phonons in the case with the GGA due to the usual overestimated bond distances as compared to LDA. The phonon dispersion for $CsSbSe_2$ was calculated previously [9] using LDA, however, its thermal properties were not explored. A convergence threshold for energy was set to 10^{-8} eV and 10^{-8} eV/Å for the interatomic forces. We used a 2×2×2 supercell for calculating harmonic force constants (IFCs) using VASP-phonopy [47] and anharmonic IFCs using VASP-thirdorder.py[48]. We calculated κ by solving the space- and time-dependent Boltzmann transport equation for phonons as implemented in almaBTE[52] and ShengBTE[53]. An 8×8×8 Monkhorst Pack grid was used for structure optimization while a 4×4×4 K-grid was used for calculation of IFCs. We used a 36×36×36 K-grid for electronic and electron transport calculations. Electron transport properties were calculated using BoltzTraP[49].

Supporting Information: Supporting Information associated with this manuscript includes phase diagrams, mean square displacements and additional lattice dynamical properties for Cs_3SbSe_4 and $CsSbSe_2$ including phonon dispersions using LDA and GGA functional forms.

Corresponding Author: SM:saikatrel@gmail.com, TLR:tom.reinecke@nrl.navy.mil

Author Contributions:

S.M designed the research, performed the calculations, analyzed the results and wrote the paper.

TLR and DJS discussed the results and contributed to the analysis and writing of the manuscript.

Notes

The authors declare no competing financial interests.

Acknowledgements: This work was supported by the Office of Naval Research. Calculations were done using the HPC Modernization Program. This research was performed while SM was a NRC Research Associate at Naval Research Laboratory.

References

1. Chang, C. & Zhao, L. D. Anharmoncity and low thermal conductivity in thermoelectrics. *Materials Today Physics* **2018**, *4*, 50–57.

2. Zhang, Y. *et al.* First-principles description of anomalously low lattice thermal conductivity in thermoelectric Cu-Sb-Se ternary semiconductors. *Physical Review B - Condensed Matter and Materials Physics* **2012**, *85*, 054306.

3. Tan, G., Zhao, L. D. & Kanatzidis, M. G. Rationally Designing High-Performance Bulk Thermoelectric Materials. *Chemical Reviews* **2016**, *116*, 12123–12149.

4. He, J. *et al.* Bi2PdO4: A Promising Thermoelectric Oxide with High Power Factor and Low Lattice Thermal Conductivity. *Chemistry of Materials* **2017**, *29*, 2529–2534.

5. Zhang, D. *et al.* Ternary CuSbSe2 chalcostibite: Facile synthesis, electronic-structure and thermoelectric performance enhancement. *Journal of Materials Chemistry A* **2016**, *4*, 4188–4193.

6. Skoug, E. J. & Morelli, D. T. Role of lone-pair electrons in producing minimum thermal

conductivity in nitrogen-group chalcogenide compounds. *Physical Review Letters* **2011**, *107*, 235901.

7. Mukhopadhyay, S. & Reinecke, T. L. Lone-Pair Electron-Driven Thermoelectrics at Room Temperature. *Journal of Physical Chemistry Letters* **2019**, *10*, 4117–4122.

8. Dutta, M., Pal, K., Waghmare, U. V. & Biswas, K. Bonding heterogeneity and lone pair induced anharmonicity resulted in ultralow thermal conductivity and promising thermoelectric properties in n-type AgPbBiSe3. *Chemical Science* **2019**, *10*, 4905–4913.

9. Nielsen, M. D., Ozolins, V. & Heremans, J. P. Lone pair electrons minimize lattice thermal conductivity. *Energy and Environmental Science* **2013**, *6*, 570–578.

10. Rathore, E. *et al.* Origin of Ultralow Thermal Conductivity in n-Type Cubic Bulk AgBiS 2 : Soft Ag Vibrations and Local Structural Distortion Induced by the Bi 6s 2 Lone Pair. *Chemistry of Materials* **2019**, *31*, 2106–2113.

11. Du, B., Zhang, R., Chen, K., Mahajan, A. & Reece, M. J. The impact of lone-pair electrons on the lattice thermal conductivity of the thermoelectric compound CuSbS2. *Journal of Materials Chemistry A* **2017**, *5*, 3249–3259.

12. Lai, W., Wang, Y., Morelli, D. T. & Lu, X. From bonding asymmetry to anharmonic rattling in Cu12Sb4S13 tetrahedrites: When lone-pair electrons are not so lonely. *Advanced Functional Materials* **2015**, *25*, 3648–3657.

13. Jana, M. K., Pal, K., Waghmare, U. V. & Biswas, K. The Origin of Ultralow Thermal Conductivity in InTe: Lone-Pair-Induced Anharmonic Rattling. *Angewandte Chemie - International Edition* **2016**, *55*, 7792–7796.

14. Feng, Z., Jia, T., Zhang, J., Wang, Y. & Zhang, Y. Dual effects of lone-pair electrons and rattling atoms in CuBiS2 on its ultralow thermal conductivity. *Physical Review B* **2017**, *96*, 235205.

15. Lin, Z. *et al.* Thermal conductivities in NaSnAs, NaSnP, and NaSn2As2: Effect of double lone-pair electrons. *Physical Review B* **2017**, *95*, 165201.

16. Fabini, D. H. *et al.* Dynamic Stereochemical Activity of the Sn2+ Lone Pair in Perovskite CsSnBr3. *Journal of the American Chemical Society* **2016**, *138*, 11820–11832.

17. Fu, Y. & Singh, D. J. Thermal conductivity of perovskite KTaO3 and PbTiO3 from first principles. *Physical Review Materials* **2018**, *2*, 094408.

18. Pal, K., Xia, Y., He, J. & Wolverton, C. High thermoelectric performance in BaAgYTe3 via low lattice thermal conductivity induced by bonding heterogeneity. *Physical Review Materials* **2019**, *3*, 085402.

19. Grin, Y. Inhomogeneity and anisotropy of chemical bonding and thermoelectric properties of materials. *Journal of Solid State Chemistry* **2019**, *274*, 329–336.

20. Li, X. *et al.* Ultralow thermal conductivity from transverse acoustic phonon suppression in distorted crystalline α-MgAgSb. *Nature Communications* **2020**, *11*, 942.

21. Mukhopadhyay, S. *et al.* The curious case of cuprous chloride: Giant thermal resistance and anharmonic quasiparticle spectra driven by dispersion nesting. *Physical Review B* **2017**, *96*, 100301.

22. Chen, X. *et al.* Twisting phonons in complex crystals with quasi-one-dimensional substructures. *Nature Communications* **2015**, *6*, 6723.

23. Lee, S. *et al.* Resonant bonding leads to low lattice thermal conductivity. *Nature Communications* **2014**, *5*, 3525.

24. Wang, H. *et al.* Lone-Pair Electrons Do Not Necessarily Lead to Low Lattice Thermal Conductivity: An Exception of Two-Dimensional Penta-CN2. *Journal of Physical Chemistry Letters* **2018**, *9*, 2474–2483.

25. Li, R. *et al.* High-Throughput Screening for Advanced Thermoelectric Materials: Diamond-Like ABX2 Compounds. *ACS Applied Materials and Interfaces* **2019**, *11*, 24859–24866.

26. Jain, A. *et al.* Commentary: The materials project: A materials genome approach to accelerating materials innovation. *APL Materials* **2013**, *1*, 011002.

27. Krause, O., Näther, C. & Bensch, W. Cs3NbSe4. *Acta Crystallographica Section C: Crystal Structure Communications* **1999**, *55*, 1197–1199.

28. Kanishcheva, A.S.; Mikhailov, Yu.N.; Moshchalkova, N.A.; Lazarev, V. B. The crystal structure of CsSbSe2. *Doklady Akademii Nauk SSSR* **1980**, *252*, 872–875.

29. Duda, J. C., Hopkins, P. E., Shen, Y. & Gupta, M. C. Exceptionally low thermal conductivities of films of the fullerene derivative PCBM. *Physical Review Letters* **2013**, *110,* 015902.

30. Wang, X., Liman, C. D., Treat, N. D., Chabinyc, M. L. & Cahill, D. G. Ultralow thermal conductivity of fullerene derivatives. *Physical Review B - Condensed Matter and Materials Physics* **2013**, *88,* 075310.

31. Chen, C. *et al.* Zintl-phase Eu 2 ZnSb 2 : A promising thermoelectric material with ultralow thermal conductivity. *Proceedings of the National Academy of Sciences of the United States of America* **2019**, *116*, 2831–2836.

32. Sootsman, J. R., Chung, D. Y. & Kanatzidis, M. G. New and Old Concepts in Thermoelectric Materials. *Angewandte Chemie International Edition* **2009**, *48*, 8616–8639.

33. Ren, W., Geng, H., Zhang, Z. & Zhang, L. Filling-Fraction Fluctuation Leading to Glasslike Ultralow Thermal Conductivity in Caged Skutterudites. *Physical Review Letters* **2017**, *118,* 245901.

34. Sales, B. C., Mandrus, D. & Williams, R. K. Filled Skutterudite Antimonides: A New Class of Thermoelectric Materials. *Science* **1996**, ***272,*** 1325–1328.

35. Takabatake, T., Suekuni, K., Nakayama, T. & Kaneshita, E. Phonon-glass electron-crystal thermoelectric clathrates: Experiments and theory. *Reviews of Modern Physics* **2014**, *86*, 669–716.

36. Schmitt, D. C. *et al.* Probing the lower limit of lattice thermal conductivity in an ordered extended solid: Gd 117Co 56Sn 112, a phonon glass-electron crystal system. *Journal of the American Chemical Society* **2012**, *134*, 5965–5973.

37. Lin, H. *et al.* Concerted Rattling in CsAg5Te3 Leading to Ultralow Thermal Conductivity and High Thermoelectric Performance. *Angew.Chem. Int.Ed.* **2016**, *55,* 11431 –11436.

38. Morelli, D. T., Jovovic, V. & Heremans, J. P. Intrinsically minimal thermal conductivity in cubic I-V-VI2 semiconductors. *Physical Review Letters* **2008**, *101*, 035901.

39. Li, C. W. *et al.* Orbitally driven giant phonon anharmonicity in SnSe. *Nature Physics* **2015**, *11*, 1063–1069.

40. Li, C. W. *et al.* Phonon self-energy and origin of anomalous neutron scattering spectra in SnTe and PbTe thermoelectrics. *Physical Review Letters* **2014**, *112*, 175501.

41. Delaire, O. *et al.* Giant anharmonic phonon scattering in PbTe. *Nature Materials* **2011**, *10,* 614–619.

42. Robinson, K., Gibbs, G. V. & Ribbe, P. H. Quadratic elongation: A quantitative measure of distortion in coordination polyhedra. *Science* **1971**, *172*, 567–570.

43. Ioffe, A. F. & Regel, A. R. *in Progress in Semiconductors*. **4**, (Wiley, 1960).

44. Mukhopadhyay, S. *et al.* Two-channel model for ultralow thermal conductivity of crystalline Tl3VSe4. *Science* **2018**, *360*, 1455–1458.

45. Simoncelli, M., Marzari, N. & Mauri, F. Unified theory of thermal transport in crystals and glasses. *Nature Physics* **2019**, *15*, 809–813.

46. Xia, Y., Pal, K., He, J., Ozoliņš, V. & Wolverton, C. Particlelike Phonon Propagation Dominates Ultralow Lattice Thermal Conductivity in Crystalline Tl3VSe4. *Physical Review Letters* **2020**, *124*, 065901.

47. Ravichandran, N. K. & Broido, D. Unified first-principles theory of thermal properties of insulators. *Physical Review B* **2018**, *98,* 085205.

48. He, J. *et al.* Ultralow Thermal Conductivity in Full Heusler Semiconductors. *Physical Review Letters* **2016**, *117*, 046602.

49. Hu, L. *et al.* Tuning Multiscale Microstructures to Enhance Thermoelectric Performance

of n-Type Bismuth-Telluride-Based Solid Solutions. *Advanced Energy Materials* **2015**, *5,* 1500411.

50. Kresse, G. & Furthmüller, J. Efficiency of ab initio total energy calculations for metals and semiconductors using a plane wave basis set. *Comput. Mat. Sci.* **1996**, ***6***, 15.

51. Kresse, G. & Joubert, D. From ultrasoft pseudopotentials to the projector augmented - wave method. *PHYSICAL REVIEW B* **1999**, *59*, 1758.

52. Carrete, J. *et al.* almaBTE : A solver of the space–time dependent Boltzmann transport equation for phonons in structured materials. *Computer Physics Communications* **2017**, *270*, 351.

53. Li, W., Carrete, J., Katcho, N. A. & Mingo, N. ShengBTE: A solver of the Boltzmann transport equation for phonons. *Computer Physics Communications* **2014**, *185,* 1747–1758.

Table of Contents (ToC Image)

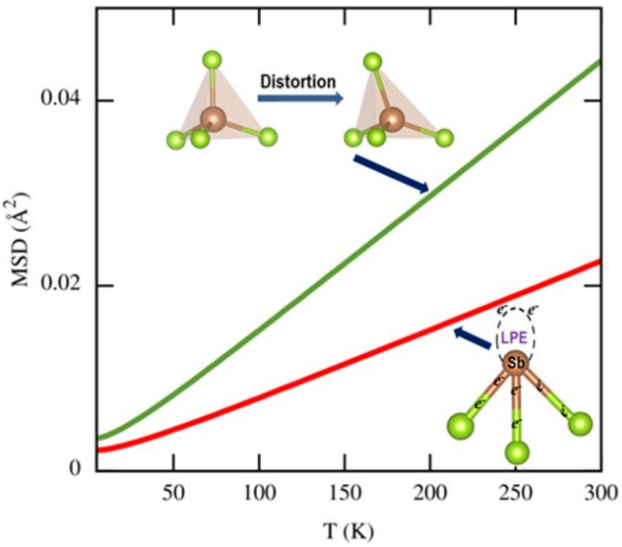

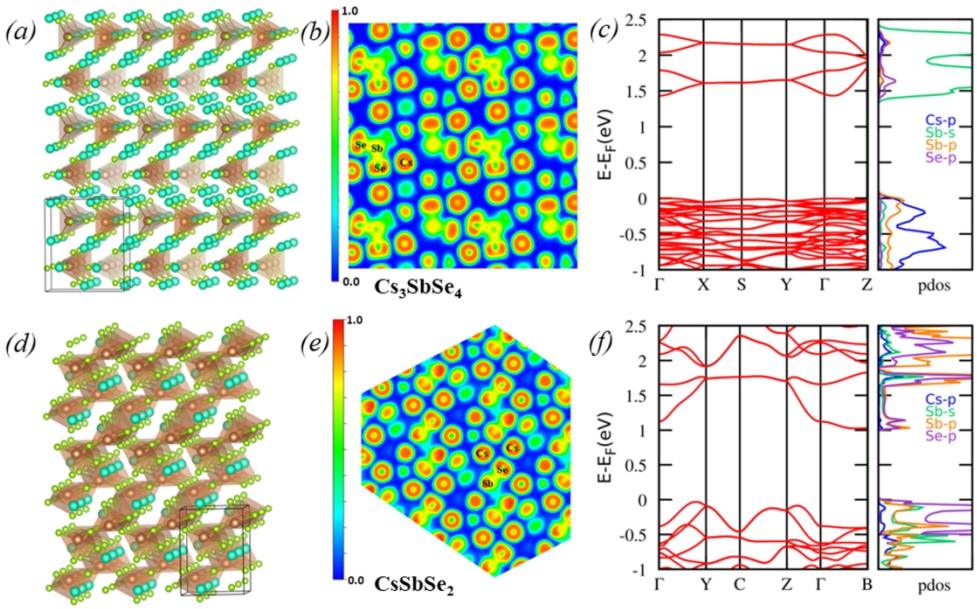

Figure 1: Structural and electronic properties: (a) and (d): 3×3×3 supercells of Cs3SbSe4 and CsSbSe2 where Cs, Sb and Se atoms are represented by aqua, orange and lime-green spheres. The corresponding unit cells are represented by boxes with solid black lines. (b) and (e): Electron localization functions projected along the [101] and [111] plane of Cs3SbSe4 and CsSbSe2. (c) and (f): Electron band structures with the density of states projected on the orbitals for Cs3SbSe4 and CsSbSe2.

177x108mm (300 x 300 DPI)

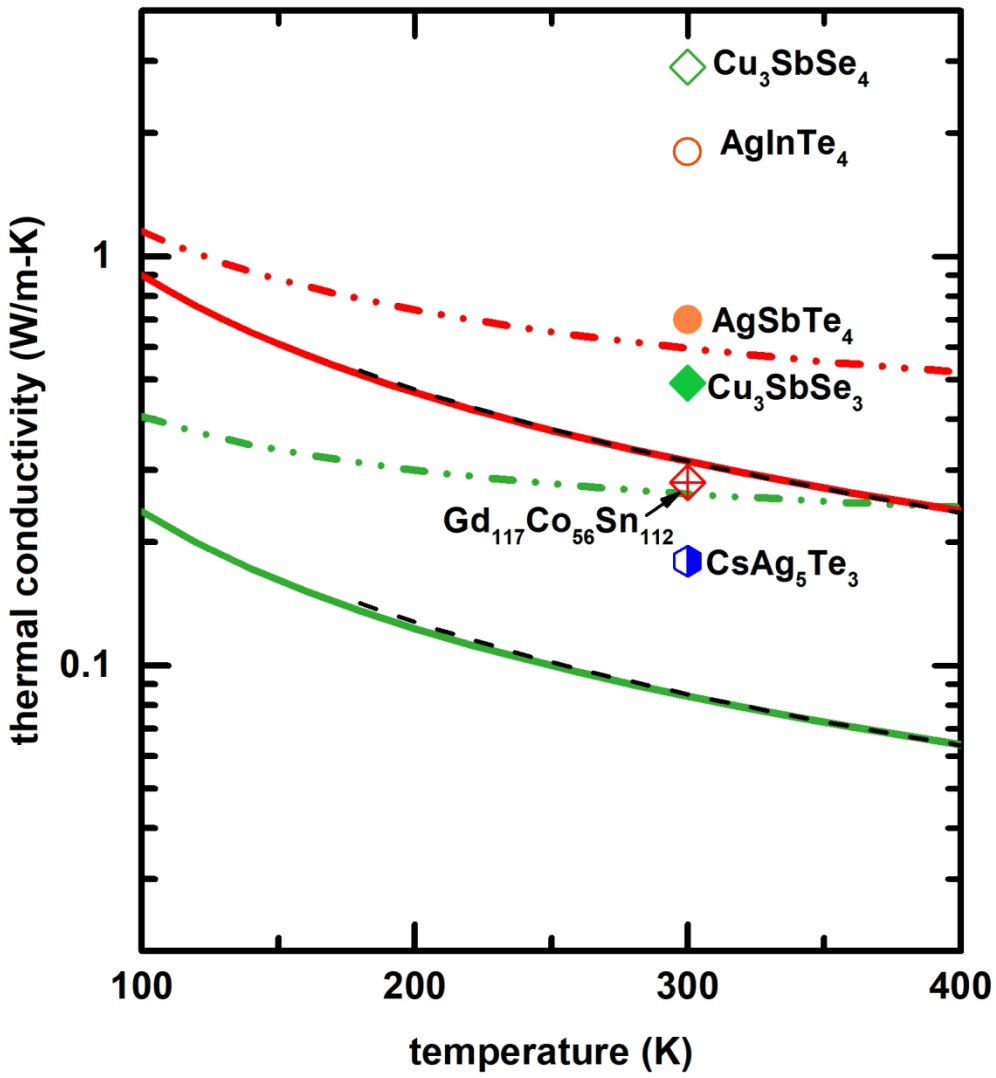

Figure 2: Calculated thermal conductivities in Cs3SbSe4 (solid green line) and CsSbSe2 (solid red line) with their corresponding T−1asymptotics (black dashed lines). The corresponding calculated thermal conductivities from the two-channel model (discussed below) are given in dashed-dotted green and red lines. The measured ☐ for Cu3SbSe3 and Cu3SbSe46, AgSbTe4 and AgInTe438 are shown as representative systems showing ☐ in systems with/without LPE. The measured ☐ for Gd117Co56Sn112 36 and CsAg5Te3 37 represents known low ☐ materials with very complex unit cells.

133x142mm (300 x 300 DPI)

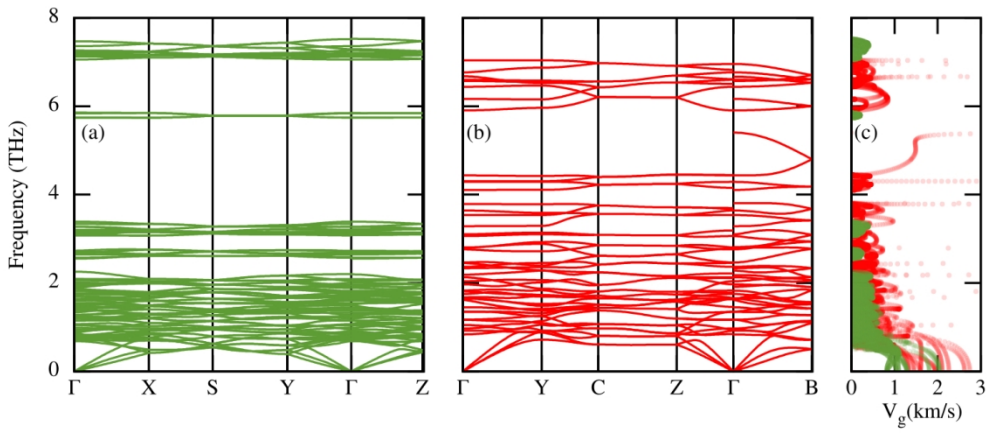

Figure 3: Phonon dispersion of (a) Cs3SbSe4 and (b) CsSbSe2. (c) Calculated average group velocities for Cs3SbSe4 (in green) and CsSbSe2 (in red).

130x56mm (300 x 300 DPI)

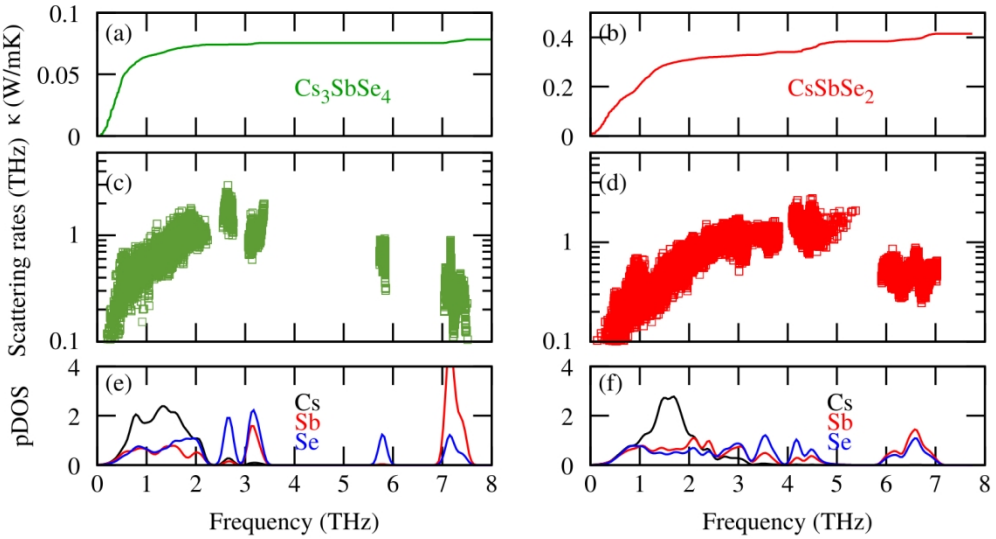

Figure 4: Accumulated □ at 300K as a function of frequency for (a) Cs3SbSe4 and (b) CsSbSe2. Scattering rates as a function of frequency for (c) Cs3SbSe4 and (d) CsSbSe2 at 300K. Phonon density of states (pDOS/atom) projected on constituent atoms for (e) Cs3SbSe4 and (f) CsSbSe2.

137x74mm (300 x 300 DPI)